Urinary Norepinephrine Excretion

Prior to the experiments, urinary norepinephrine excretion was significantly higher in SHRSP than in WKY (Fig. 3). In WKY, urinary norepinephrine excretion was significantly higher in 'jet lag'-WKY than in control-WKY at 1-2 day after the initiation of 'jet lag', and was similar in 'jet lag'-WKY and control-WKY at 3-5 day after the initiation of 'jet lag' (Fig. 3). In SHRSP, urinary Units norepinephrine excretion was significantly higher in 'jet lag'-SHRSP than in control-WKY for the period of 'jet lag' (Fig. 3).

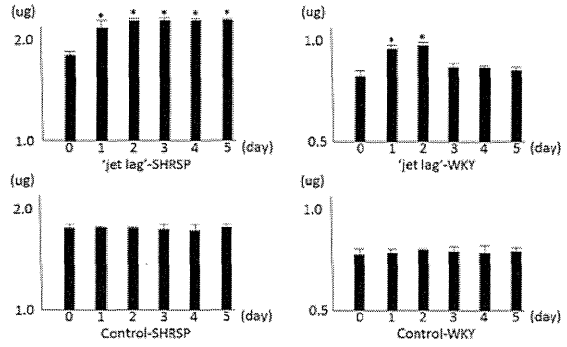

Fig 3. The results of the urinary norepinephrine excretion in each group for 5 days of jet lag. N=5 for each. *P<0.05 vs control.

Oxidative Stress in the RVLM

In WKY, TBARS in the RVLM was significantly higher in 'jet lag'-WKY than in control-WKY at 2 day after the initiation of 'jet lag', and was similar in 'jet lag'-WKY and control-WKY at 5 day after the initiation of 'jet lag' (Fig. 4). In SHRSP, TBARS in the RVLM was significantly higher in 'jet lag'-SHRSP than in control-WKY both at 2 and 5 day after the initiation of 'jet lag' (Fig. 4).

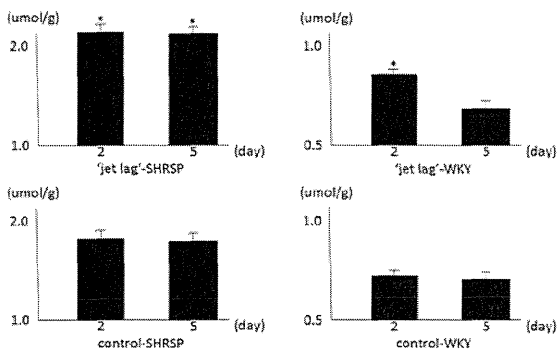

Fig 4. The results of the levels of TBARS in the RVLM of each group. N=5 for each. *P<0.05 vs control.

Microinjection of Angiotensin II Type 1 Receptor Blocker into the RVLM

In WKY, the depressor effect due to the microinjection of losartan into the RVLM was significantly greater in 'jet lag'-WKY than in control-WKY at 2 day after the initiation of 'jet lag', and was similar in 'jet lag'-WKY and control-WKY at 5 day after the initiation of 'jet lag' (Fig. 5). In SHRSP, the depressor effect was significantly greater in 'jet lag'-SHRSP than in control-WKY both at 2 and 5 day after the initiation of 'jet lag' (Fig. 5).

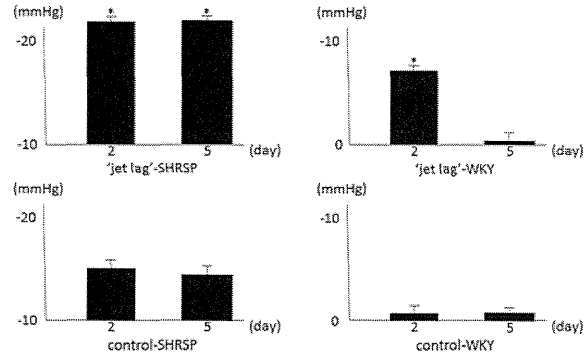

Fig 5. The results of the degree of the depressor effects due to the microinjection of losartan into the RVLM. N=5 for each. *P<0.05 vs control.

DISCUSSION

In the present study, we demonstrated that 1) in WKY, 'jet lag' increases blood pressure and the activity of sympathetic nervous system via oxidative stress through angiotensin II type 1 receptor in the RVLM for 2 days only, and the changes are improved at 3 day after the initiation of 'jet lag', 2) in SHRSP, 'jet lag' also increases blood pressure and the activity of sympathetic nervous system via oxidative stress through angiotensin II type 1 receptor in the RVLM, and the changes are maintained for the period of 'jet lag'. From these results, we consider that 'jet lag' causes sympathoexcitation via oxidative stress through angiotensin II type 1 receptor in the RVLM, and the 'jet lag'-induced sympathoexcitation is maintained and excessive in SHRSP. The clinical implications from the present study are that hypertension is a risk of 'jet lag'-induced sympathoexcitation, and that angiotensin II type 1 receptor blocker might be an effective agent of the treatment for 'jet lag'-induced sympathoexcitation.

The most important finding in the present study is that 'jet lag' activates the angiotensin II type 1 receptor in the brain. The activity of the sympathetic nervous system is regulated mainly by the angiotensin II type 1 receptor-induced oxidative stress in the RVLM [11]-[13]. Previous studies have suggested that 'jet lag' increases blood pressure [3]-[4]. Taken together, we consider that the mechanisms of 'jet lag'-induced hypertension and sympathetic activation might be due to the activation of the angiotensin II type 1 receptor in the brain. Furthermore, while the sympathoexcitation is tentative in WKY, the sympathoexcitation is maintained in SHRSP. We should consider that hypertension is a worsening factor of 'jet lag'-induced sympathoexcitation.

In terms of the treatment for 'jet lag'-induced sympathoexcitation, the target of the treatment might be angiotensin II type 1 receptor in the RVLM. To inhibit the angiotensin II type 1 receptor in the brain, in the present study, we performed the microinjection of the angiotensin II type 1 receptor blocker directly into the RVLM, and in our previous study, we performed the intracerebroventricular infusion of the angiotensin II type 1 receptor blocker [13]. In clinical aspects, oral administration of angiotensin II type 1 receptor blocker might be a novel agent, because some oral intake of angiotensin II type 1 receptor blocker affects the RVLM through the blood-brain barrier [10]. Moreover, we have also demonstrated that some other oral agents, especially statin, have the potential to inhibit the oxidative stress in the brain [10, 14]. In the further study, we should examine the effects of the oral administration of the angiotensin II type 1 receptor blocker s and / or statins on the 'jet lag'-induced sympathoexcitation.

The mechanisms in which 'jet lag' activates the angiotensin II type 1 receptor in the brain have not been determined in the present study. In hypertension, previous studies have suggested that the angiotensin II type 1 receptor in the brain is activated by the circulating angiotensin II and / or baroreflex circuit [8, 10]. In the present study, we did not determine the changes in the concentration of plasma angiotensin II and the baroreflex sensitivity. Further studies must be done to determine mechanisms in which 'jet lag' activates the angiotensin II type 1 receptor in the brain.

There are some limitations in the present study. First, we only examined the oxidative stress in the RVLM. The increase in oxidative stress in the brain of 'jet lag' may not be the unique phenomenon in the RVLM. However, in the regulation of sympathetic nerve activity, RVLM is the most important cite. Furthermore, in the RVLM, oxidative stress is the most powerful and important sympatho-exciting factor [11, 13]. From these reasons, we focused on the oxidative stress in the RVLM. Second, we did not perform the long-term RVLM-specific inhibition of AT_1 receptor. We must do the RVLM-specific knock down of AT_1 receptor in the future study.

CONCLUSION

The results from the present study suggest that experimental 'jet lag' causes sympathoexcitation via oxidative stress through AT_1 receptor in the brain, especially in hypertensive states.

APPENDIX

None.

ACKNOWLEDGEMENT

This work was supported by a Grant-in-Aid for Scientific Research from the Japan Society for the Promotion of Science (B193290231).

REFERENCES

[1] A.J. Davidson, O. C. Castanon, T. L. Leise, P. C. Molyneux, M. E. Harrington, "Visualizing jet lag in the mouse suprachiasmatic nucleus and peripheral circadian timing system", Eur J Neurosci, vol. 29, pp. 171-180, 2009.

[2] E. S. Maywood, J. O'Neill, G. K. Wong, A. B. Reddy, M. H. Hastings, "Circadian timing in health and disease", Prog Brain Res, vol. 153, pp. 253-269, 2006.

[3] M. Ha, J. Park, "Shiftwork and metabolic risk factors of cardiovascular disease", J Occup Health, vol. 47, pp. 89-95, 2005.

[4] M. Kivimaki, M. Virtanen, M. Elovainio, A. Vaananen, L. K. Jarvinen L, "Prevalent cardiovascular disease, risk factors and selection out of shift work", Scand J Work Environ Health, vol. 32, pp. 204-208, 2006.

[5] R. Y. Moore, V. B. Eichker, "Loss of a circadian adrenal corticosterone rhythm following suprachiasmatic lesions in the rat", Brain Res, vol. 42, pp. 201-206, 1972.

[6] R. Chen, A. Schirmer, Y. Lee, H. Lee, V. Kumar, "Rhythmic PER abundance defines a critical nodal point for negative feedback within the circadian clock mechanisms", Mol Cell, vol. 36, pp. 417-430, 2009.

[7] E. M. Gibson, C Wang, S Tjho, N Khattar, L.J. Kriegsfeld, "Experimental 'jet lag' inhibits adult neurogenesis and produces long-term cognitive deficits in female hamsters", PloS ONE, vol. 5, e15267, 2010.

[8] P. G. Guyenet PG, "The sympathetic control of blood pressure", Nat Rev Neurosci, vol. 7. pp. 335-346, 2006.

[9] Y. Hirooka, K. Sakai, T. Kishi, A. Takeshita, "Adenovirus-mediated gene transfer into the NTS in conscious rats: A new approach to examining the central control of cardiovascular regulation", Ann N Y Acad Sci, vol. 940, pp. 197-205, 2001.

[10] Y. Hirooka, T. Kishi, K. Sakai, A. Takeshita, K. Sunagawa, "Imbalance of central nitric oxide and reactive oxygen species in the regulation of sympathetic activity and neural mechanisms of hypertension", Am J Physiol, vol. 300, pp. R818-R826, 2011.

[11] T. Kishi, Y. Hirooka, Y. Kimura, K. Ito, H. Shimokawa, A. Takeshita, "Increased reactive oxygen species in rostral ventrolateral medulla contribute to neural mechanisms of hypertension in stroke-prone spontaneously hypertensive rats", Circulation, vol. 109, pp. 2357-2362, 2004.

[12] M. Nozoe, Y. Hirooka, Y. Koga, S. Araki, S. Konno, T. Kishi, T. Ide, K. Sunagawa K, "Mitochondria-derived reactive oxygen species mediate sympathoexcitation induced by angiotensin II in the rostral ventrolateral medulla", J Hypertens, vol. 26, pp. 2176-2184, 2008.

[13] T. Kishi, Y. Hirooka, S. Konno, K. Ogawa, K. Sunagawa, "Angiotensin II type 1 receptor-activated caspase-3 through ras/mitgen-activated protein kinase-extracellular signal-regulated kinase in the rostral ventrolateral medulla is involved in sympathoexcitation in stroke-prone spontaneously hypertensive rats", Hypertension, vol. 55, pp. 291-294, 2010.

[14] T. Kishi, Y. Hirooka, H. Shimokawa, A. Takeshita, K. Sunagawa, "Atorvastatin reduces oxidative stress in the rostral ventrolateral medulla of stroke-prone spontaneously hypertensive rats", Clin Exp Hypertens, vol. 30, pp. 1-9, 2008.

33rd Annual International Conference of the IEEE EMBS
Boston, Massachusetts USA, August 30 - September 3, 2011

Artificial Baroreflex System Restores Volume Tolerance in the Absence of Native Baroreflex

Kazuya Hosokawa, Kouta Funakoshi, Atsushi Tanaka, Takafumi Sakamoto, Ken Onitsuka, Kazuo Sakamoto, Tomoyuki Tobushi, Takeo Fujino, Keita Saku, Yoshinori Murayama, Tomomi Ide and Kenji Sunagawa, *Senior Member, IEEE*

***Abstract*— The arterial baroreflex stabilizes arterial pressure by modulating the mechanical properties of cardiovascular system. We previously demonstrated that the baroreflex impairment makes the circulatory system extremely sensitive to volume overload and predisposes to pulmonary edema irrespective of left ventricular systolic function. To overcome the volume intolerance, we developed an artificial baroreflex system by directly stimulating the carotid sinus nerves in response to changes in arterial pressure. The artificial baroreflex system precisely reproduced the native arterial pressure response and restored physiological volume buffering function. We conclude that the artificial baroreflex system would be an attractive tool in preventing pulmonary edema in patients with impaired baroreflex function.**

I. Introduction

Heart failure is a major medical problem worldwide. Although latest therapeutic strategy benefits many patients with heart failure, their prognosis remains unacceptably poor [1]. We demonstrated that baroreflex failure induces volume intolerance and predisposes to pulmonary edema irrespective of left ventricular systolic function. At present, no therapeutic strategy to restore baroreflex function is available. The aim of this study is to develop an artificial baroreflex system capable of restoring volume buffering function.

Manuscript received April 15, 2011. This work was supported in part by Health and Labour Sciences Research Grant for Research on Medical Devices for Improving Impaired QOL from the Ministry of Health Labour and Welfare of Japan, Health and Labour Sciences Research Grant for Clinical Research from the Ministry of Health Labour and Welfare of Japan, and Grant-in-Aid for Scientific Research(S) (18100006) from the Japan Society for the Promotion of Science

Authors are with Kyushu University Graduate School of Medical Sciences, Department of Cardiovascular Medicine. 8128582 Higashi-ku, Maidashi 3-1-1, Fukuoka, Japan (corresponding author K. Hosokawa to provide phone: +81-92-642-5360; fax: +81-92-642-5357; e-mail: ncvchoso@cardiol.med.kyushu-u.ac.jp).

II. Methods

Surgical Preparations

The care and use of the animals were strict accordance with the guiding principles of our institution. In 14 anesthetized Sprague-Dawley rats weighing 562±37g, the baroreceptor regions were vascularily isolated [2]. The intra-carotid sinus pressure (CSP) was controlled by a servo-controlled piston pump (ET-126A and PA-119; Labworks, Costa Mesa, CA). Bilateral aortic depressor nerves were cut and a pair of electrodes was attached to the proximal end of the aortic depressor nerves for stimulation.

Framework of the artificial baroreflex system

As shown in Fig. 1, the artificial baroreflex system consisted of a pressure sensor, regulator and neuro-stimulator. The operating rule (H_{ABS}), how the regulator translates arterial pressure (AP) into stimulation (STM), was identified by the ratio of transfer functions from CSP to AP ($H_{CSP\text{-}AP}$) to that from STM to AP ($H_{STM\text{-}AP}$). To obtain $H_{CSP\text{-}AP}$ and $H_{STM\text{-}AP}$, we perturbed CSP and the pulse frequency of the neuro-stimulation with random binary sequences (Data were not shown).

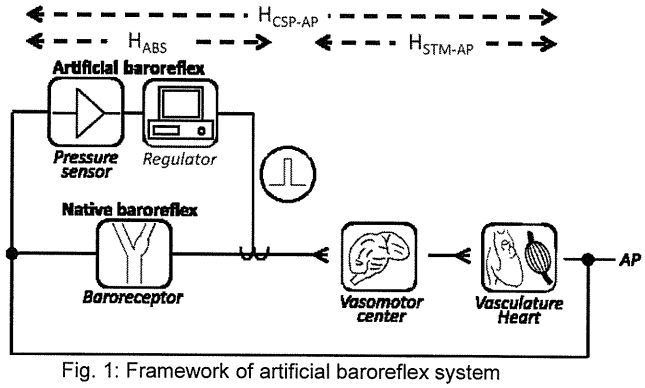

Fig. 1: Framework of artificial baroreflex system

A. Protocol-1: Comparison of open-loop pressure regulation between the native baroreflex and artificial baroreflex system

We implemented identified H_{ABS} into the regulator. Under the open loop condition (Fig. 2), we alternatively imposed pressure changes stepwise into CSP and the pressure sensor of the artificial baroreflex system. We then compared the arterial pressure responses.

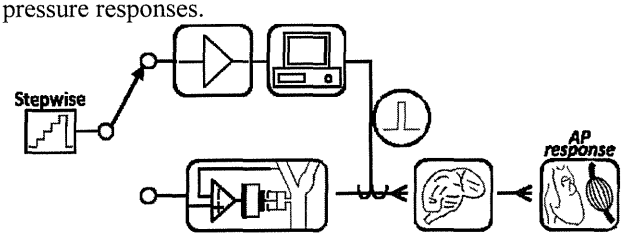

Fig. 2: Comparison of open-loop pressure regulation between the native baroreflex and artificial baroreflex system (Protocol -1)

B. Protocol-2: Comparison of volume buffering function between the native baroreflex and artificial baroreflex system

Under the closed loop condition of the native or artificial baroreflex system (Fig. 3), in order to examine the volume buffering function, we infused dextran stepwise and measured left atrial pressure (LAP) every 1 minute until LAP reaches 11mmHg. We plotted the LAP-infused volume relationships.

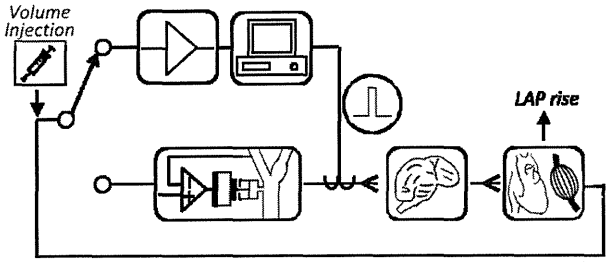

Fig. 3: Comparison of volume buffering function between the native baroreflex and artificial baroreflex system (Protocol-2)

III. RESULTS

Identification of the H_{ABS}

Both H_{CSP-AP} and H_{STM-AP} showed the characteristics of lowpass filter with similar corner frequencies. Taking the ratio of H_{CSP-AP} to H_{STM-AP} yielded H_{ABS} (Data were not shown).

A. Protocol-1: Comparison of open-loop pressure regulation between the native baroreflex and artificial baroreflex system

The arterial pressure responses between the native baroreflex and artificial baroreflex system were indistinguishable (Fig. 4). Maximal gain was -2.28±0.88 in the native baroreflex and was -2.20±1.18 (NS, n=7) in the artificial baroreflex system.

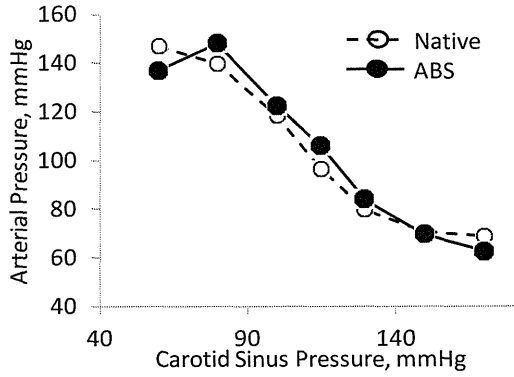

Fig. 4: The artificial baroreflex system reproduces the native baroreflex function

B. Protocol-2: Comparison of volume buffering function between the native baroreflex and artificial baroreflex system

In comparison with no baroreflex, the native baroreflex markedly buffered the increase in LAP in response to volume infusion. The artificial baroreflex system was as powerful as the native baroreflex in buffering the increase in LAP to volume infusion (Fig. 5).

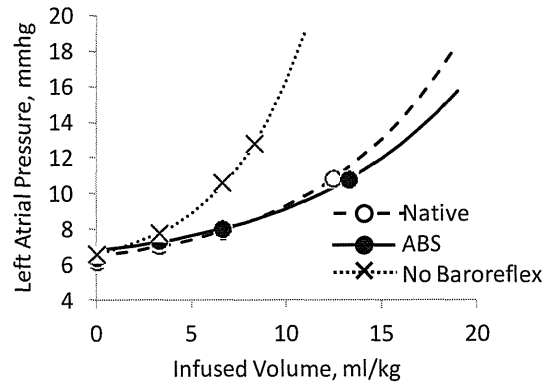

Fig. 5: The artificial baroreflex system restores normal volume buffering function

IV. DISCUSSION

We have shown that the artificial baroreflex system reproduced the open-loop characteristics of baroreflex pressure regulation reasonably well including the saturation and threshold effects of native baroreflex (Fig. 4). Since electrical stimulation of the carotid sinus nerves is linearly dependent on input arterial pressure (CSP), the reproduction of the nonlinear pressure responses would like to reflect the nonlinear sympathetic activation by the central mechanism.

The artificial baroreflex system restored physiological volume buffering function (Fig. 5). We estimated the amount of volume required to induce pulmonary edema by fitting the LAP-infused volume relationship to a monoexponential curve. We defined the critical volume load (critical ΔV) at which LAP reaches 18mmHg. The critical volume was 21.0±3.0ml/kg in the artificial baroreflex system and 20.1±3.0ml/kg in the native baroreflex, compared with 16.6 ± 4.4ml/kg in no baroreflex. The critical ΔV was markedly increased in normal baroreflex and in the artificial baroreflex system.

V. Conclusion

The artificial baroreflex system fully restored volume buffering function as well as arterial pressure regulation. The artificial baroreflex system would be an attractive therapeutic tool in preventing pulmonary edema in the presence of baroreflex failure irrespective of left ventricular systolic function. In order to develop a clinically useful system, further inventions in developing durable pressure sensors and electrodes are essential [3].

Acknowledgment

This study was supported in part by Health and Labour Sciences Research Grant for Research on Medical Devices for Improving Impaired QOL from the Ministry of Health Labour and Welfare of Japan, Health and Labour Sciences Research Grant for Clinical Research from the Ministry of Health Labour and Welfare of Japan, and Grant-in-Aid for Scientific Research(S) (18100006) from the Japan Society for the Promotion of Science.

References

[1] Owan TE, Hodge DO, Herges RM, Jacobsen SJ, Roger VL, Redfield MM. Trends in prevalence and outcome of heart failure with preserved ejection fraction. The New England journal of medicine. 2006;355(3):251-259.

[2] Sato T, Kawada T, Miyano H, Shishido T, Inagaki M, Yoshimura R, Tatewaki T, Sugimachi M, Alexander J, Jr., Sunagawa K. New simple methods for isolating baroreceptor regions of carotid sinus and aortic depressor nerves in rats. The American journal of physiology. 1999;276(1 Pt 2):H326-332.

[3] Sugimachi M, Sunagawa K. Bionic Cardiology: Exploration Into a Wealth of Controllable Body Parts in the Cardiovascular System. IEEE REVIEWS IN BIOMEDICAL ENGINEERING. 2009:2:172-186.

厚生労働省科学研究補助金
医療技術実用化総合研究事業

平成２０年度～平成２４年度
総合研究報告書

慢性心不全の予後を改善するための非侵襲で安全・安心な無痛性ICDの実用化臨床試験
（Ｈ２０－活動－指定－００７）

主任研究者：砂川　賢二
（九州大学大学院医学研究院）

Vol. 3

平成２５（２０１３）年５月

厚生労働省科学研究補助金
医療技術実用化総合研究事業

平成２０年度～平成２４年度
総合研究報告書

慢性心不全の予後を改善するための非侵襲で安全・安心な無痛性ICDの実用化臨床試験
（Ｈ２０－活動－指定－００７）

主任研究者：砂川　賢二
（九州大学大学院医学研究院）

Vol. 3

平成２５（２０１３）年５月

目　　次
Vol. 3

33rd Annual International Conference of the IEEE EMBS
Boston, Massachusetts USA, August 30 - September 3, 2011

Consideration on Step Duration to Assess Open-loop Static Characteristics of the Carotid Sinus Baroreflex in Rats

Toru Kawada, Shuji Shimizu, Yusuke Sata, Atsunori Kamiya, Kenji Sunagawa, and Masaru Sugimachi

Abstract—**The carotid sinus baroreflex is one of the most important negative feedback systems to stabilize arterial pressure. Although static characteristics of the carotid sinus baroreflex can be assessed by using a stepwise input protocol under baroreflex open-loop conditions, the step duration has been determined empirically. In the present study, we examined the effects of different time windows (5-10, 15-20, 25-30, 35-40, 45-50, and 55-60 s) on the static characteristics estimated by using a 60-s stepwise input protocol in 10 anesthetized rats. Based on the results, we compared the static characteristics between actual 60-s and 20-s stepwise input protocols. Most of the parameters of the static characteristics did not differ significantly between the 60-s and 20-s stepwise input protocols, suggesting that the open-loop baroreflex static characteristics can be estimated by using a stepwise input with the step duration as short as 20 s in normal rats.**

I. Introduction

The carotid sinus baroreflex system is one of the most important negative feedback systems to stabilize arterial pressure (AP). The carotid sinus baroreflex may be divided into two principal subsystems [1], [2]. One is a neural arc subsystem that acts as a controller for regulating sympathetic nerve activity (SNA) in response to a baroreceptor pressure input. The other is a peripheral arc subsystem that serves as a plant for yielding AP according to SNA through cardiovascular responses. In order to assess the open-loop static characteristics of these two subsystems, a stepwise (staircase-wise) input has been employed. The levels of input pressure are changed stepwise to cover the whole input pressure range of the arterial baroreflex, e.g., between 60 and 180 mmHg in rats. Each input pressure level is sustained for certain duration to make the system response reach steady state at a given input pressure level. Empirically, 60-s step duration seems to be appropriate for estimating the baroreflex static characteristics in rats [3], [4]. Although minimizing the step duration would contribute to shortening the total experimental time, too short duration can violate the assumption of acquiring the steady-state response. In the present study, we examined possible shortest step duration necessary for estimating the baroreflex open-loop static characteristics in rats.

Manuscript received March 20, 2011. This work was supported in part by Health and Labour Sciences Research Grants (H19-nano-Ippan-009, H20-katsudo-Shitei-007, H21-nano-Ippan-005) from the Ministry of Health, Labour and Welfare of Japan.

T. Kawada, S. Shimizu, Y. Sata, and M. Sugimachi are with the Department of Cardiovascular Dynamics, National Cerebral and Cardiovascular Center, 565-8565 Osaka, Japan (corresponding author: T. Kawada, phone: +81-6-6833-5012, fax: +81-6-6835-5403, e-mail: torukawa@res.ncvc.go.jp).

K. Sunagawa is with the Department of Cardiovascular Medicine, Graduate School of Medical Sciences, Kyushu University, Fukuoka 812-8582, Japan.

II. Materials and Methods

A. Animal Preparation

Animals were cared for in strict accordance with the *Guiding Principles for the Care and Use of Animals in the Field of Physiological Sciences*, which has been approved by the Physiological Society of Japan. All experimental protocols were reviewed and approved by the Animal Subjects Committee at National Cerebral and Cardiovascular Center.

The study was conducted using ten male Sprague-Dawley rats. Each rat was anesthetized by an intraperitoneal injection (2 ml/kg) of a mixture of urethane (250 mg/ml) and α-chloralose (40 mg/ml), and mechanically ventilated through a tracheal tube with oxygen-enriched room air. A venous catheter was inserted into the right femoral vein for a maintenance dose of the above anesthetic mixture diluted by 20 fold (2-3 $ml \cdot kg^{-1} \cdot h^{-1}$). An arterial catheter was inserted into the right femoral artery to measure AP, from which heart rate (HR) was detected. Another venous catheter was inserted into the left femoral vein for the infusion of Ringer solution (6 $ml \cdot kg^{-1} \cdot min^{-1}$) to maintain fluid balance.

In order to record SNA, a postganglionic branch from the splanchnic sympathetic nerve was exposed through a left flank incision. A pair of stainless steel wire electrodes (Bioflex wire, AS633, Cooner Wire, CA, USA) was attached to the nerve, and the nerve and electrodes were covered with silicone glue (Kwik-Sil, World Precision Instruments, FL, USA). To quantify the nerve activity, the preamplified signal was band-pass filtered at 150-1000 Hz, and was full-wave rectified and low-pass filtered with a cut-off frequency of 30 Hz. Pancuronium bromide (0.4 $mg \cdot kg^{-1} \cdot h^{-1}$) was administered to prevent muscular activity from contaminating the SNA recording. At the end of the experiment, an intravenous bolus injection of a ganglionic blocker, hexamethonium bromide (60 mg/kg), was given to confirm the disappearance of SNA. The noise level was then recorded and served as zero SNA. Because the absolute magnitude of SNA varied among animals depending on recording conditions, mean SNA value corresponding to the carotid sinus pressure (CSP) of 60 mmHg calculated at the time window of 55-60 s was assigned to be 100 au (arbitrary units).

Bilateral vagal and aortic depressor nerves were sectioned at the neck to avoid reflexes from the cardiopulmonary region

and aortic arch. The carotid sinus regions were isolated from the systemic circulation using previously reported procedures [5], [6] with modifications. A 7-0 polypropylene suture with a fine needle (PROLENE, Ethicon, GA, USA) was passed through the tissue between the external and internal carotid arteries, and the external carotid artery was ligated close to the carotid bifurcation. The internal carotid artery was embolized by the injection of two to three steel balls with a diameter of 0.8 mm (Tsubaki Nakashima, Nara, Japan) via the common carotid artery. The isolated carotid sinuses were filled with warmed Ringer solution via the catheter inserted into the common carotid arteries. CSP was controlled using a servo-controlled piston pump. Heparin sodium (100 U/kg) was given intravenously to prevent blood coagulation. Body temperature was maintained at approximately 38°C with a heating pad and a lamp.

B. Estimation of Baroreflex Open-loop Static Characteristics Using Different Time Windows in a 60-s Stepwise Input

To estimate the open-loop static characteristics of the total baroreflex, neural arc, peripheral arc, and HR control, CSP was first decreased to 60 mmHg for four min, and increased stepwise from 60 to 180 mmHg at increments of 20 mmHg every minute.

Mean values of SNA, AP, and HR were calculated from time windows of 5-10, 15-20, 25-30, 35-40, 45-50, and 55-60 s at each CSP level. In each rat, data from two consecutive 60-s stepwise input cycles were averaged. The static characteristics of the total baroreflex (the CSP-AP relationship), neural arc (the CSP-SNA relationship), and HR control (the CSP-HR relationship) were quantified using a four-parameter logistic function as [7]:

$$y = \frac{P_1}{1+\exp[P_2(x-P_3)]} + P_4$$

where x and y denote the input and output values, respectively; P_1 is the response range; P_2 is the slope coefficient, P_3 is the midpoint input pressure; and P_4 is the minimum value of the output.

The static characteristics of the baroreflex peripheral arc (the SNA-AP relationship) were quantified by a linear regression analysis as:

$$AP = a \times SNA + b$$

where a and b represent the slope and intercept, respectively.

C. Estimation of Baroreflex Open-loop Static Characteristics Using a 20-s Stepwise Input

Based on preliminary results of the open-loop static characteristics using different time windows in a 60-s stepwise input described above, the system response to a 20-s stepwise input was examined. The 20-s stepwise input protocol was conducted before (n = 5) or after (n = 5) the 60-s stepwise input protocol to make the possible time effect be even between the two protocols. Mean values of SNA, AP, and HR were obtained during the last 5 s (15-20 s) at each CSP level. In each rat, data from two consecutive 20-s stepwise input cycles were averaged.

D. Statistical Analysis

All data are expressed as means±SE values. To compare the effects of differing the time windows of analysis (5-10, 15-20, 25-30, 35-40, 45-50, and 55-60 s) on the parameters of the baroreflex static characteristics, repeated-measures analysis of variance (ANOVA) was used [8]. If there was a significant difference, a Dunnett's test was applied to identify the difference against the data calculated from a time window of 55-60 s. To compare the parameters of the baroreflex static characteristics between the 60-s and 20-s stepwise input protocols, a paired-t test was used. Differences were considered to be significant when $P < 0.05$. We used a rule of thumb that the parameters derived from two protocols were considered to be similar when $P > 0.2$.

III. Results and Discussion

Fig. 1 represents typical recordings of CSP, SNA, AP, and HR during 60-s and 20-s stepwise input protocols. A white line in the SNA recording is a 2-s moving averaged signal. An increase in CSP decreased SNA, AP, and HR. The maximum and minimum values of SNA, AP, and HR responses did not differ significantly between the two input protocols.

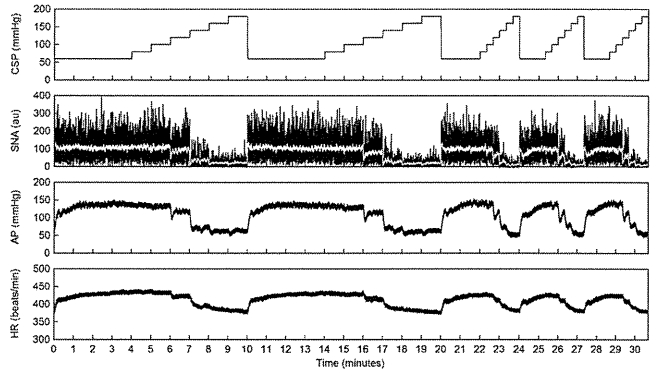

Fig. 1. Typical experimental recordings during 60-s and 20-s stepwise input protocols. CSP: carotid sinus pressure, SNA: sympathetic nerve activity, AP: arterial pressure, HR: heart rate. The white line in the SNA recording represents a 2-s moving averaged signal.

Figure 2 (the last page) summarizes the open-loop static characteristics of the total baroreflex, neural arc, peripheral arc, and HR control, obtained from the 60-s stepwise input protocol, with the analyses using different time windows. The characteristics of the total baroreflex, neural arc, and HR control approximated an inverse sigmoid curve. The characteristics of the peripheral arc approximated a straight line. The data obtained during 55-60 s served as controls. The estimated parameter values, except those estimated during 5-10 s, did not differ significantly from those obtained during 55-60 s (Table 1), suggesting that the open-loop static characteristics of the baroreflex could be obtained using a stepwise input with step duration as short as 20 s.

Figure 3 (the last page) compares the open-loop static characteristics of the total baroreflex, neural arc, peripheral arc, and HR control between actually applied 20-s and 60-s stepwise input protocols. Data were calculated from the last 5 s of each step. The lines of mean data obtained from the two protocols were very close (Fig. 3, right panels, dashed line: 20-s, solid line: 60-s). In the parameters of the total baroreflex, no significant differences were detected between the two protocols (Table 2). In the neural arc, although the slope coefficient was significantly smaller by 0.006 in the 20-s stepwise input protocol, the magnitude of the difference was comparable to the corresponding SE value (0.006) in the 60-s stepwise input protocol. Other parameters of the neural arc did not differ significantly. Parameters of the peripheral arc did not differ significantly between the two protocols. In the HR control, although the response range was significantly smaller by 3.6 beats/min in the 20-s stepwise input protocol, the magnitude of the difference was less than the corresponding SE value (7.5 beats/min) in the 60-s stepwise input protocol. Other parameters did not differ significantly. Although we did not carry out an equivalence test, if we use a rule of thumb that the two parameter values are considered to be similar when $P > 0.2$, the midpoint input pressure (P_3) could be different in all of the total baroreflex, neural arc, and the HR control. The percent difference of P_3 values relative to the value estimated by the 60-s stepwise input protocol was, however, less than 5% on the average. Collectively, although several parameters differed slightly, the 20-s stepwise input protocol provided parameter values similar to those obtained from the 60-s stepwise input protocol. The differences of the parameters between the two protocols could not be detected if we applied an unpaired-t test instead of a paired-t test, suggesting that the detected difference was within the inter-individual variations.

Although too short step duration in a stepwise input protocol will violate the assumption that the system's steady-state response is obtained, too long step duration will also violate the assumption that the system remains stationary. Minimizing the step duration may contribute to shortening the total experimental time and making the assumption for stationarity more feasible in biological experiment. In addition, when examining the effects of certain interventions on the system characteristics, reducing the step duration would increase the time resolution for tracking the effects of interventions on the system characteristics. In other words, by using a 20-s stepwise input protocol, we may be able to increase the time resolution of the systems analysis by 3 fold compared to a 60-s stepwise input protocol.

There is a limitation to the present study. We estimated the baroreflex static characteristics in normal anesthetized rats. In diseased conditions such as chronic heart failure, the cardiovascular responses could be blunted [3]. In such conditions, longer step duration may be required for AP to reach a new steady state at a given input pressure, and thus the 20-s stepwise input protocol may not work well. Apparently, some priori knowledge or preliminary studies are needed to use the 20-s rather than the 60-s stepwise input protocol.

IV. Conclusion

The open-loop static characteristics of the carotid sinus baroreflex in normal rats may be obtained by the stepwise input protocol with step duration as short as 20 s. The shortening of the step duration can reduce the total amount of experimental time. Moreover, it would also make it possible to analyze the time effect of drugs on the baroreflex static characteristics with a better time resolution.

References

[1] D. E. Mohrman, L. J. Heller. Cardiovascular Physiology, 6th ed. New York: Lange Medical Books/McGraw-Hill, 2006, pp. 172–177.

[2] T. Sato, T. Kawada, M. Inagaki, T. Shishido, H. Takaki, M. Sugimachi, et al. "New analytic framework for understanding sympathetic baroreflex control of arterial pressure," *Am. J. Physiol.*, vol. 276, pp. H2251-H2261, 1999.

[3] T. Kawada, M. Li, A. Kamiya, S. Shimizu, K. Uemura, H. Yamamoto, et al. "Open-loop dynamic and static characteristics of the carotid sinus baroreflex in rats with chronic heart failure after myocardial infarction," *J. Physiol. Sci.*, vol. 60, pp. 283-298, 2010.

[4] T. Kawada, A. Kamiya, M. Li, S. Shimizu, K. Uemura, H. Yamamoto, et al. "High levels of circulating angiotensin II shift the open-loop baroreflex control of splanchnic sympathetic nerve activity, heart rate and arterial pressure in anesthetized rats," *J. Physiol. Sci.*, vol. 59, pp. 447-455, 2010.

[5] A. A. Shoukas, C. A. Callahan, J. M. Lash, E. B. Haase. "New technique to completely isolate carotid sinus baroreceptor regions in rats," *Am. J. Physiol. Heart Circ. Physiol.*, vol. 260, pp. H300-H303, 1991.

[6] T. Sato, T. Kawada, H. Miyano, T. Shishido, M. Inagaki, R. Yoshimura, et al. "New simple methods for isolating baroreceptor regions of carotid sinus and aortic depressor nerves in rats," *Am. J. Physiol. Heart Circ. Physiol.*, vol. 276, pp. H326-H332, 1999.

[7] B. B. Kent, J. W. Drane, B. Blumenstein, J. W. Manning. "A mathematical model to assess changes in the baroreceptor reflex," *Cardiology.*, vol. 57, pp. 295-310, 1972.

[8] S. A. Glantz, Primer of Biostatistics, 5th ed. New York: McGraw-Hill, 2002, pp. 318-329.

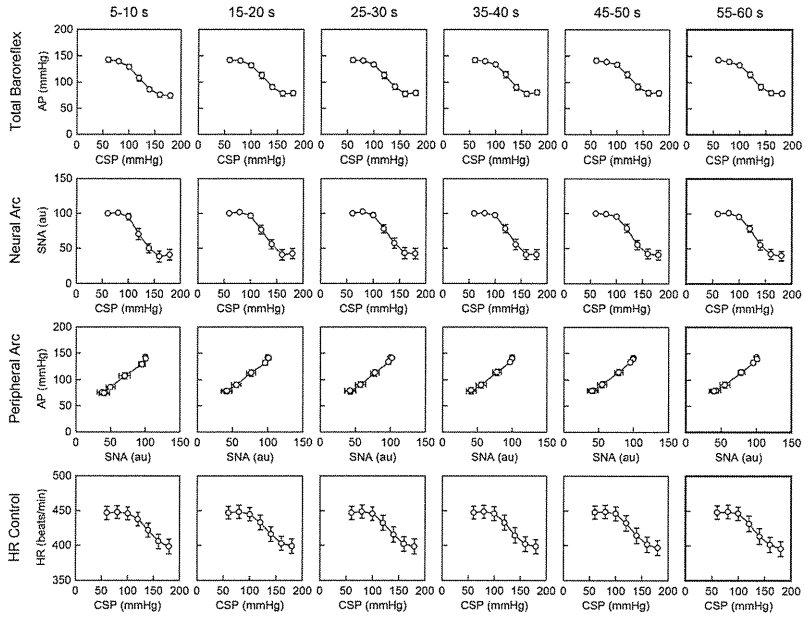

Fig. 2. Open-loop static characteristics of the carotid sinus baroreflex estimated at different time windows of the 60-s stepwise input protocol. CSP: carotid sinus pressure, AP: arterial pressure, SNA: sympathetic nerve activity, HR: heart rate. The rightmost panels serve as controls.

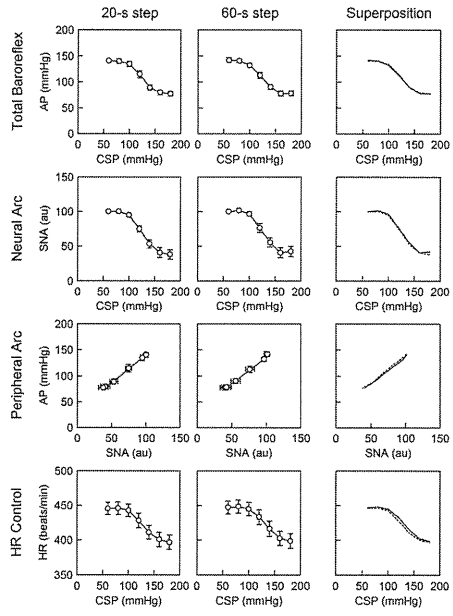

Fig. 3. Open-loop static characteristics of the carotid sinus baroreflex estimated using 20-s and 60-s stepwise input protocols. CSP: carotid sinus pressure, AP: arterial pressure, SNA: sympathetic nerve activity, HR: heart rate.

Table 1. Parameters of open-loop static characteristics of the carotid sinus baroreflex estimated at different time windows in the 60-s stepwise input protocol.

	5-10 s	15-20 s	25-30 s	35-40 s	45-50 s	55-60 s
Total Baroreflex						
P_1, mmHg	72.5±8.6**	68.8±8.0	67.9±7.8	66.4±7.7	65.0±7.8	65.4±7.1
P_2, mmHg^{-1}	0.088±0.011	0.089±0.009	0.095±0.011	0.099±0.009	0.097±0.009	0.091±0.008
P_3, mmHg	118.1±3.6**	122.1±3.5	122.8±3.6	123.6±3.5	124.0±3.6	123.7±3.6
P_4, mmHg	72.9±4.8**	74.9±5.2	75.1±5.2	75.5±5.1	76.2±5.1	76.3±4.8
Neural Arc						
P_1, au	65.5±7.6	63.0±6.7	62.6±8.0	62.8±7.3	61.3±7.1	63.1±6.5
P_2, mmHg^{-1}	0.115±0.014	0.102±0.012	0.102±0.010	0.100±0.009	0.101±0.010	0.088±0.006
P_3, mmHg	120.6±3.6**	125.1±3.7	126.0±3.8	127.8±3.8	127.2±3.6	127.0±3.6
P_4, au	37.6±7.8	39.3±7.4	40.1±8.1	38.4±7.3	39.3±7.1	38.7±6.7
Peripheral Arc						
a, mmHg/au	1.06±0.07	1.06±0.07	1.10±0.07	1.09±0.08	1.07±0.07	1.06±0.07
b, mmHg	31.0±7.4	31.2±6.9	27.0±8.0	29.4±8.1	32.0±6.4	32.1±7.0
HR Control						
P_1, beats/min	52.8±8.2	51.8±8.4	52.3±8.2	51.7±8.0	53.8±8.0	54.8±7.5
P_2, mmHg^{-1}	0.077±0.006	0.082±0.008	0.089±0.010	0.093±0.009	0.087±0.008	0.083±0.007
P_3, mmHg	138.5±2.9**	131.0±3.1	131.0±3.4	130.5±3.3	131.1±3.6	130.8±3.5
P_4, beats/min	395.7±10.8	397.2±10.4	396.8±10.8	397.4±10.3	395.7±10.6	395.2±10.5

Data are means±SE values. **P < 0.01 by Dunnett's test from the value estimated at a time window of 55-60 s.

Table 2. Parameters of open-loop static characteristics of the carotid sinus baroreflex estimated by actual 20-s and 60-s stepwise input protocols.

	20-s step	60-s step	P value	%difference
Total Baroreflex				
P_1, mmHg	65.9±7.5	65.4±7.1	0.779	0.1±3.5
P_2, mmHg^{-1}	0.094±0.009	0.091±0.008	0.691	1.0±8.1
P_3, mmHg	121.9±3.0	123.7±3.6	0.148	1.4±0.9
P_4, mmHg	76.6±4.3	76.3±4.8	0.893	−0.4±2.0
Neural Arc				
P_1, au	65.5±7.6	63.1±6.5	0.330	−1.5±4.5
P_2, mmHg^{-1}	0.082±0.008*	0.088±0.006	0.011	10.8±3.8
P_3, mmHg	121.8±3.3	127.0±3.6	0.075	4.4±2.3
P_4, au	37.4±7.2	38.7±6.7	0.414	9.6±7.5
Peripheral Arc				
a, mmHg/au	1.09±0.08	1.06±0.07	0.351	−1.1±2.5
b, mmHg	31.4±8.3	32.1±7.0	0.780	7.3±11.1
HR Control				
P_1, beats/min	51.2±8.2*	54.8±7.5	0.041	13.7±7.6
P_2, mmHg^{-1}	0.082±0.008	0.083±0.007	0.820	6.6±8.9
P_3, mmHg	126.5±3.3	130.8±3.5	0.126	3.5±2.1
P_4, beats/min	396.4±10.4	395.2±10.5	0.501	−0.3±0.4

Data are means±SE values. *P < 0.05 by a paired-t test.

Original Article

Imatinib Mesylate-Incorporated Nanoparticle-Eluting Stent Attenuates In-Stent Neointimal Formation in Porcine Coronary Arteries

Seigo Masuda[1], Kaku Nakano[1], Kouta Funakoshi[1], Gang Zhao[2], Wei Meng[2], Satoshi Kimura[3], Tetsuya Matoba[1], Miho Miyagawa[1], Eiko Iwata[1], Kenji Sunagawa[1] and Kensuke Egashira[1]

[1]Department of Cardiovascular Medicine, Graduate School of Medical Sciences, Kyushu University, Fukuoka, Japan
[2]Department of Cardiovascular Medicine, 6th People's Hospital, Shanghai Jiatong University, Shanghai, China
[3]Department of Cardiovascular Surgery, Graduate School of Medical Sciences, Kyushu University, Fukuoka, Japan

Aim: The use of currently marketed drug-eluting stents (DES) presents safety concerns, including an increased risk for late thrombosis in the range of 0.6% per year in patients, including acute coronary syndrome, which is thought to result from delayed endothelial healing effects. A new DES system targeting vascular smooth muscle cells without adverse effects on endothelial cells is therefore needed. Platelet-derived growth factor (PDGF) plays a central role in the pathogenesis of restenosis; therefore, we hypothesized that imatinib mesylate (PDGF receptor tyrosine kinase inhibitor) encapsulated bioabsorbable polymeric nanoparticle (NP)-eluting stent attenuates in-stent neointima formation.
Methods: Effects of imatinib-incorporated NP-eluting stent on neointima formation and endothelial healing were examined in a pig coronary artery stent model. Effects of imatinib-NP were also examined in cultured cells.
Results: In a cultured cell study, imatinib-NP attenuated the proliferation of vascular smooth muscle cells associated with inhibition of the target molecule (phosphorylation of PDGF receptor-β), but showed no effect on endothelial proliferation. In a pig coronary artery stent model, imatinib-NP-eluting stent markedly attenuated in-stent neointima formation and stenosis by approximately 50% as assessed by angiographic, histopathological, and intravascular ultrasound imaging analyses. Imatinib-NP-eluting stent also attenuated MAP kinase activity, but did not affect inflammation and re-endothelialization.
Conclusion: These data suggest that suppression of neointima formation by a imatinib-NP-eluting stent holds promise as a molecular-targeting NP delivery system for preventing in-stent restenosis.

J Atheroscler Thromb, 2011; 18:1043-1053.

Key words; Nanotechnology, Drug delivery system, Restenosis, Stents, Smooth muscle cells

Introduction

Although polymer-coated drug-eluting stents (DES) can reduce restenosis and target-vessel revascularization to rates below 10% by its anti-proliferative effects on vascular smooth muscle cells (VSMC), increased risk of late in-stent thrombosis resulting in acute coronary syndrome (unstable angina, acute myocardial infarction and death) after the use of DES devices has become a major safety concern[1-3]. These adverse effects are thought to result mainly from delayed healing effects of the drugs or polymers on endothelial cells leading to impaired arterial healing processes (impaired endothelial regeneration, excessive inflammation, proliferation and fibrin deposition)[4-6]. Cell-specific molecular targeting against VSMC proliferation without negative effects on endothelial cells,

Address for correspondence: Kensuke Egashira, Department of Cardiovascular Medicine, Graduate School of Medical Science, Kyushu University, 3-1-1, Maidashi, Higashi-ku, Fukuoka 812-8582, Japan
E-mail: egashira@cardiol.med.kyushu-u.ac.jp
Received: January 20, 2011
Accepted for publication: July 1, 2011

therefore, is an essential requirement to develop more efficient and safer DES in the future.

Platelet-derived growth factor (PDGF), expressed by VSMC, plays a central role in the pathogenesis of restenosis. Mechanical forces, such as stent-induced overstretch, stimulate VSMC expression and release of PDGF in animals[7, 8] and humans[9, 10]. Imatinib mesylate is an inhibitor for c-Abl tyrosine kinase, c-Kit receptor kinase, and PDGF receptor tyrosine kinase[11, 12] and is approved for the treatment of patients with chronic myeloid leukemia. It has been shown that c-Kit-positive progenitor cells can differentiate into α-actin-positive VSMCs and may contribute to neointima formation[13]. It has also been reported that c-Abl tyrosine kinase is involved in angiotensin II-induced VSMC hypertrophy[14]. Imatinib is reported to be a significantly more potent inhibitor of VSMC proliferation than other inhibitors of PDGF receptor (AGL-2043), with $IC_{50} < 10$ nM[15]. In contrast, imatinib has little effect on vascular endothelial cell growth factor receptor tyrosine kinase or endothelial cell proliferation[15]. These data provide a rationale for the use of imatinib mesylate in the prevention of neointima formation associated with in-stent restenosis as a VSMC-specific molecular-targeting drug.

Prior studies have reported that systemic oral administration of imatinib inhibited balloon injury-induced neointima formation in rats[11] when dosages beyond the clinical norm were used (50 mg/kg per day). In contrast, imatinib had no effect on in-stent neointima formation in rabbits when administered at a clinically relevant dosage (10 mg/kg per day)[16]. Recent clinical studies in humans have detected no beneficial effects of the oral administration of imatinib (600 mg/day for 10 days)[17] on in-stent restenosis. These data suggest that systemic administration of imatinib at clinical dosages may not be sufficient to antagonize PDGF-induced vascular responses. Furthermore, it was reported the polymer-coated stents with imatinib (600 μg/stent) had no effect on neointima formation in a porcine coronary in-stent stenosis model[15]. This was probably because of unsuitable release characteristics of imatinib from polymer-coated stents. It is suggested that the present polymer coating DES technology is not useful for coating water-soluble drugs such as imatinib. Therefore, preventing in-stent restenosis via imatinib-mediated PDGF-R signaling blockade requires a new efficient drug delivery system. We previously succeeded in developing bioabsorbable polymeric nanoparticles (NP) formulated from the polymer poly (DL-lactide-co-glycolide) (PLGA)[18], and in formulating a NP-eluting stent by cation electrodeposition coating technology[19]. This NP-eluting stent system provided an effective means of delivering NP-incorporated drugs or genes that target intracellular proteins involved in the pathogenesis of in-stent neointima formation.

Therefore, we hypothesized that imatinib-NP-eluting stent can be an innovative therapeutic strategy for preventing in-stent neointima formation *in vivo*. We used a porcine coronary artery in-stent stenosis model and investigated whether imatinib-NP-eluting stent attenuates in-stent neointima formation without adverse effects on arterial healing processes *in vivo*.

Materials and Methods

Vascular Smooth Muscle Cell Proliferation Assay

Human coronary artery VSMCs (Lonza, Walkersville, MD, USA) were cultured and placed into 48-well culture plates (5000 cells per well; BD). Proliferation was stimulated by the addition of PDGF at 10 ng/mL (Sigma, Tokyo, Japan)[20]. Various concentration of imatinib (Novartis Pharma) at 0.1, 1, and 10 μM, imatinib-loaded PLGA NP (PLGA at 0.5 mg/mL containing imatinib at 10 μM), or vehicle alone was added to the wells, and four days later, the cells were fixed with methanol and a single observer counted the number of cells/plate.

Endothelial Cell Proliferation Assay

Human umbilical vein endothelial cells (HUVEC) were obtained, cultured, and used between passages 4 to 8[21]. Recombinant human VEGF165 (10 ng/mL; R&D) or PDGF at 10 ng/mL was added to the basal medium, and cells (7500 cells per well) were incubated in the presence or absence of imatinib, imatinib-NP, or vehicle for 4 days in 48-well culture plates. Cell count assay was performed as stated above.

Preparation of NP-Eluting Stents by Cationic Electrodeposition Coating Technology

A lactide/glycolide copolymer (PLGA) with an average molecular weight of 20,000 and a lactide to glycolide copolymer ratio of 75:25 (PLGA7520; Wako Pure Chemical Industries, Osaka, Japan) was used as wall material for the NP. Chitosan was used to coat the surface of PLGA NP. Polyvinylalcohol (PVA-403; Kuraray, Osaka, Japan) was used as a dispersing agent. PLGA NP incorporated with the fluorescent marker fluorescein isothiocyanate (FITC; Dojindo laboratories, Kumamoto, Japan) or with imatinib (purchased from a pharmacy) were prepared by a previously reported emulsion solvent diffusion method in purified water[19, 22, 23].

The mean particle size was analyzed by the light

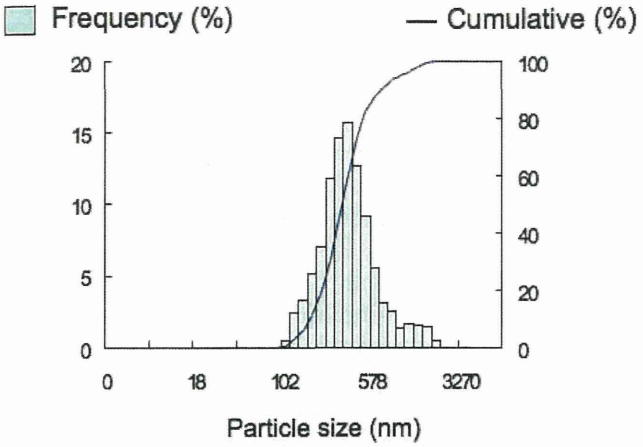

Fig. 1. Particle size distribution of imatinib-incorporated PLGA nanoparticles in water.

scattering method (Microtrack UPA150; Nikkiso, Tokyo, Japan). A sample of nanoparticulate suspension in distilled water was used for particle size analysis. The average diameter of FITC- and imatinib-incorporated NP was about 200 nm. Size distribution was similar between FITC-NP and imatinib-NP (see **Fig. 1**). FITC- and imatinib-encapsulated PLGA NP contained 5.0% (w/w) FITC and 8.3% (w/w) imatinib, respectively. The zeta potential of the NP as measured by Zetasizer Nano Z (Malverm, America) was +6.7 and +10.0 mV, respectively.

The 16 mm-long stainless-steel, balloon-expandable stents (Multilink) were ultrasonically cleaned in acetone, ethanol, and demineralized water. The cationic electrodeposited coating was prepared on cathodic stents in NP solution at a concentration of 5 g/L in distilled water with a current maintained between 2.0 and 10.0 mA by a direct current power supply (DC power supply; Nippon Stabilizer Co, Tokyo, Japan) for different periods under sterile conditions[19]. The coated stents were then rinsed with demineralized water and dried under a vacuum overnight. This electrodeposition coating procedure produced a coating of approximately 250 ± 40 μg of the polymer NP per stent and 21 ± 8 μg of imatinib per stent (n=12). The surface of some NP-coating stents were observed with scanning electron microscopy (JXM8600; JEOL, Tokyo, Japan).

Prior to experimental use, non-coated bare metal and NP-coated stents were mounted mechanically over the 3-mm balloon for implantation in the coronary artery. These balloon-mounted stent sets were sterilized using ethylene oxide.

Animal Preparation and Stent Implantation

All *in vivo* experiments were reviewed and approved by the Committee on Ethics in Animal Experiments, Kyushu University Faculty of Medicine, according to the Guidelines of the American Physiological Society. This study also conforms to the Guide for the Care and Use of Laboratory Animals published by the US National Institutes of Health (NIH Publication No. 85-23, revised 1996).

Domestic male pigs (Kyudo, Tosu, Japan; aged 2 to 3 months and weighing 25 to 30 kg) received oral aspirin (330 mg/day) and ticlopidine (200 mg/day) until euthanasia from 3 days before the stent implantation procedure. Animals were anesthetized with ketamine hydrochloride (15 mg/kg, IM) and pentobarbital (20 mg/kg, IV). They were then intubated and mechanically ventilated with room air. A preshaped Judkins catheter was inserted into the carotid artery and advanced to the orifice of the left coronary artery. After systemic heparinization (100 IU/kg) and intracoronary administration of nitroglycerin, coronary angiography of the left coronary artery was performed using contrast media (iopamidol 370®) in a left oblique view with an angiography system (Toshiba Medical, Tokyo, Japan). Animals were divided into 3 groups, which underwent deployment of either a non-coated bare metal stent (2 week; n=4 for Western blot analysis, 4 week; n=10 for angiographic, histopathological and intravascular ultrasound analyses), FITC-incorporated NP-eluting stents (4 week; n=10 for angiographic, histopathological and intravascular ultrasound analyses), or imatinib-incorporated NP-eluting stents (2 week; n=4 for Western blot analysis, 4 week; n=10 for angiographic, histopathological and intravascular ultrasound analyses), to either the left anterior descending (LAD) or the left circumflex coronary (LCx) arteries.

A segment with a mean coronary diameter of 2.5 mm was selected by using quantitative coronary angiography (Toshiba Medical, Tokyo, Japan) with a stent-to-artery ratio of approximately 1.1 to 1.2 (**Table 1**). A balloon catheter mounted with a stent was then advanced to the pre-selected coronary segments for deployment over a standard guidewire. The balloon catheter was inflated at 12 atm for 60 seconds once and thereafter deflated, and was then slowly withdrawn, leaving the stent in place.

Quantitative coronary angiography (Toshiba Medical, Tokyo, Japan) was performed before, immediately after, and 4 weeks after stent implantation to examine the coronary arterial diameter at stented and non-stented sites. An image of a Judkins catheter was used as the reference diameter. Arterial pressure, heart

rate, and ECG were continuously monitored and recorded on a recorder.

Intravascular Ultrasound

Intravascular ultrasound imaging (IVUS) was performed to assess the extent of neointima formation *in vivo* 4 weeks after stent implantation. Imaging was performed using a 40 MHz ultrasonic imaging catheter (Ultra cross; Boston Scientific, Boston, USA) and an automatic pullback device, and the studies were recorded on 1/2-inch high-resolution s-VHS tapes for off-line volumetric assessment. Because of the limited availability of IVUS probes, IVUS was performed 7 and 8 pigs in FITC-NP and imatinib-NP stent groups, respectively.

Histopathological Study

Four weeks after the coronary angiographic study, animals were euthanized with a lethal dose of sodium pentobarbital (40 mg/kg intravenously), and histological analysis was performed. The left coronary artery was perfused with 10% buffered formalin at 120 mm Hg and fixed for 24 hours. The stented artery segments were isolated and processed as described previously[24]: The segment was cut at the center of the stent and embedded in methyl methacrylate mixed with n-butyl methacrylate to allow for sectioning through the metal stent struts. Serial sections were stained with elastica van Gieson and with hematoxylin-eosin (HE). The neointimal area, the area within the internal elastic lamina (IEL), and the lumen area were measured by computerized morphometry, which was carried out by a single observer who was blinded to the experimental protocol. All images were captured by an Olympus microscope equipped with a digital camera (HC-2500) and were analyzed using Adobe Photoshop 6.0 and Scion Image 1.62 Software. The injury, inflammation, and re-endothelialization scores were determined at each strut site, and mean values were calculated for each stented segment[25].

Western Blot Analysis

For *in vitro* study, protein was extracted from cultured VSMC, and protein expression was analyzed using antibodies against human PDGF receptor-β (0.1 mg/mL; R&D Systems Inc.), phospho-PDGF receptor-β (0.5 mg/mL; R&D), or anti-actin (Sigma).

For *in vivo* study, animals were euthanized with a lethal dose of sodium pentobarbital (40 mg/kg intravenously) two weeks after stent implantation when the neointima was modestly formed, and Western blot analysis was performed. Protein was extracted from frozen arterial tissues excised from stented coronary arterial segments (LAD or LCx) and non-stented normal coronary arterial segments (right coronary artery). Cell extracts (20 μg) were resolved on 10% reducing SDS-PAGE gels and blotted onto nitrocellulose membranes (Bio-Rad, Hercules, CA). Protein expression was analyzed using antibodies against MAP kinase (ERK1/2) (0.5 mg/mL; R&D Systems Inc.), phosho-ERK1/2 (1:2000; Cell Signaling), or anti-actin (Sigma). Immune complexes were visualized with horseradish peroxidase-conjugated secondary antibodies (Pierce, Rockford, IL) using the ECL Plus system (Amersham Biosciences). Western blot analysis was performed with sequential antibodies and was detected with the ECL Detection Kit (Amersham).

Statistical Analysis

Data are expressed as the means ± SE. Statistical analysis of differences between two groups was performed with the unpaired *t*-test, and the statistical analysis of differences among three or more groups was assessed using ANOVA and multiple comparison tests. *P* values < 0.05 were considered significant.

Results

In vitro Effects of Imatinib on Proliferation of Vascular Smooth Muscle Cells and Endothelial Cells

We previously reported (1) the *in vitro* time course of FITC release from FITC-incorporated NP, and (2) highly efficient and stable delivery of NP into the cytoplasm of SMC and endothelial cells[19, 21, 26, 27]. In the present study, we examined *in vitro* effects of imatinib and imatinib-NP. As reported by others[15], imatinib attenuated the PDGF-induced proliferation of human coronary arterial SMC in a dose-dependent manner (**Fig. 2A**). Imatinib-NP also prevented the PDGF-induced responses of SMC. Western blot analysis showed that in human coronary artery SMC, both imatinib and imatinib-NP inhibited PDGF-induced phosphorylation of PDGF receptor-β in a dose-dependent manner (**Fig. 2B**). In contrast, neither imatinib nor imatinib-NP affected VEGF- and PDGF-induced proliferation of human endothelial cells (**Fig. 2C**).

Effects of Imatinib-NP-Eluting Stent on Neointima Formation 4 Weeks After Stent Implantation

Three animals (2 in control bare metal stent group and 1 in FITC-NP-eluting stent group) died suddenly between weeks 3 and 4; therefore, these animals were excluded from angiographic and histopathological analyses. These analyses were performed in 27

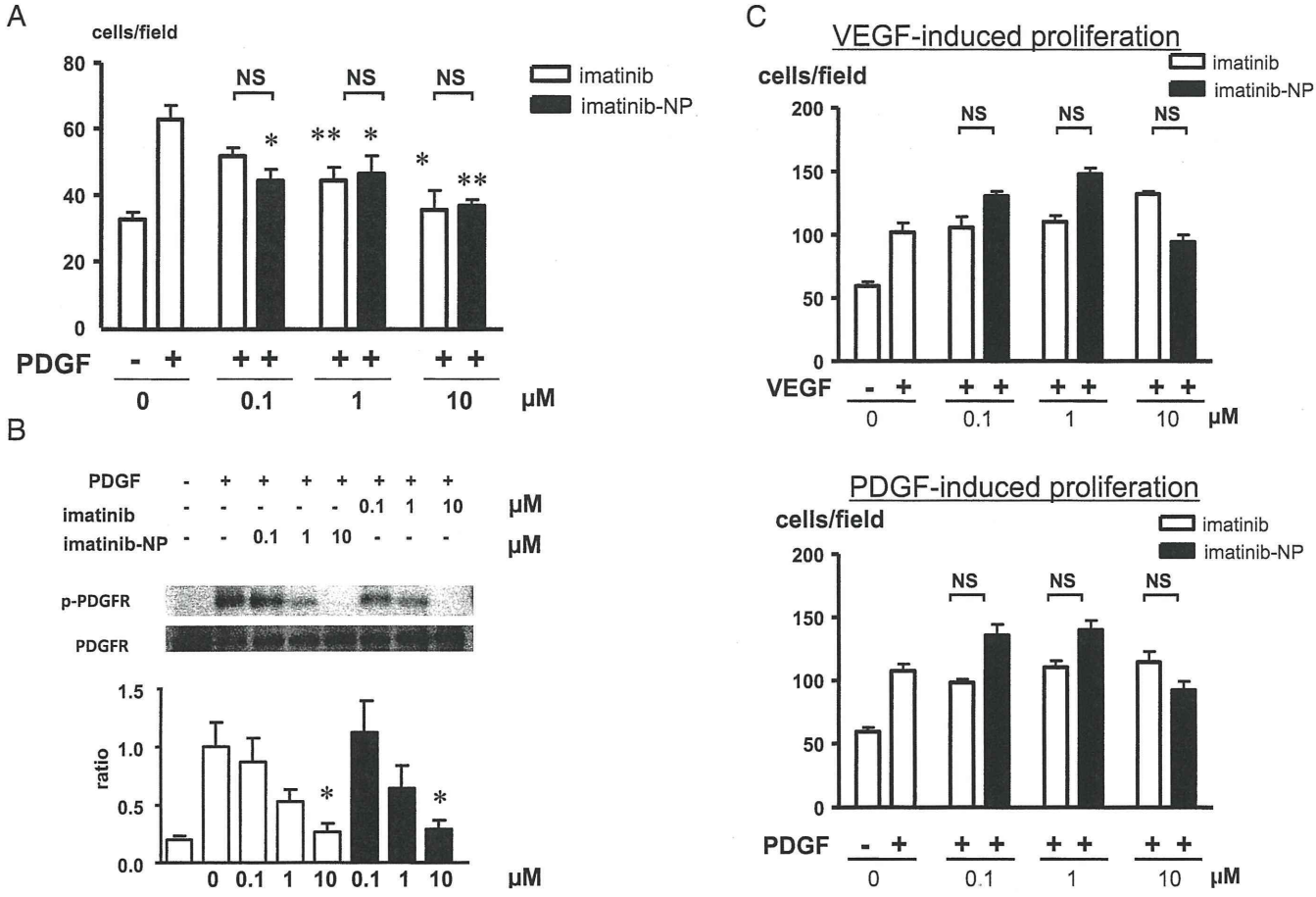

Fig. 2.

A, Effects of imatinib and imatinib-NP on PDGF-induced proliferation of human coronary artery SMCs. Data are the mean ± SEM ($n = 8$ each). $^{*}p < 0.001$ versus PDGF-induced response by two-way ANOVA and Dunnett's multiple comparison tests.
B, Effects of imatinib and imatinib-NP on PDGF-induced activation (phosphorylation) of PDGF receptor-β in human coronary artery SMC. Densitometric analysis of protein expression (p-PDGFR/PDGFR ratio) is also shown as a bar graph ($n = 5$ each). $^{*}p < 0.05$ versus the PDGF-induced response by one-way ANOVA and Dunnett's multiple comparison tests.
C, Effect of imatinib on the VEGF- and PDGF-induced proliferation of human umbilical vein endothelial cells ($n = 8$).

Table 1. Coronary artery diameter before, immediately after, and 4 weeks after stent implantation in porcine coronary artery

	Bare metal control stent ($n = 8$)	FITC-NP-eluting stent ($n = 9$)	imatinib-NP-eluting stent ($n = 10$)	p value
coronary diameter before stent implantation	2.21 ± 0.06	2.25 ± 0.05	2.32 ± 0.05	0.33
coronary diameter immediately after stent implantation	2.63 ± 0.08	2.65 ± 0.05	2.70 ± 0.04	0.70
stent-to-artery ratio immediately after stent implantation	1.19 ± 0.03	1.18 ± 0.03	1.17 ± 0.02	0.74
coronary diameter 4 weeks after stent implantation	1.48 ± 0.14	1.49 ± 0.12	2.06 ± 0.16	0.009

Data are the mean ± SEM. $^{*}p < 0.01$ versus coronary diameter before stent implantation, $^{\dagger}p < 0.01$ versus coronary diameter immediately after stent implantation, $^{\#}p < 0.01$ versus bare metal control stent group.

pigs (8 in control bare metal stent group, 9 in FITC-NP-eluting stent group, and 10 in imatinib-NP eluting stent group).

Quantitative coronary arteriography revealed that (1) there was no significant difference in the coronary diameter before and immediately after stent implantation and the stent-to-artery ratio among the 3 groups; and (2) the coronary diameter was less in

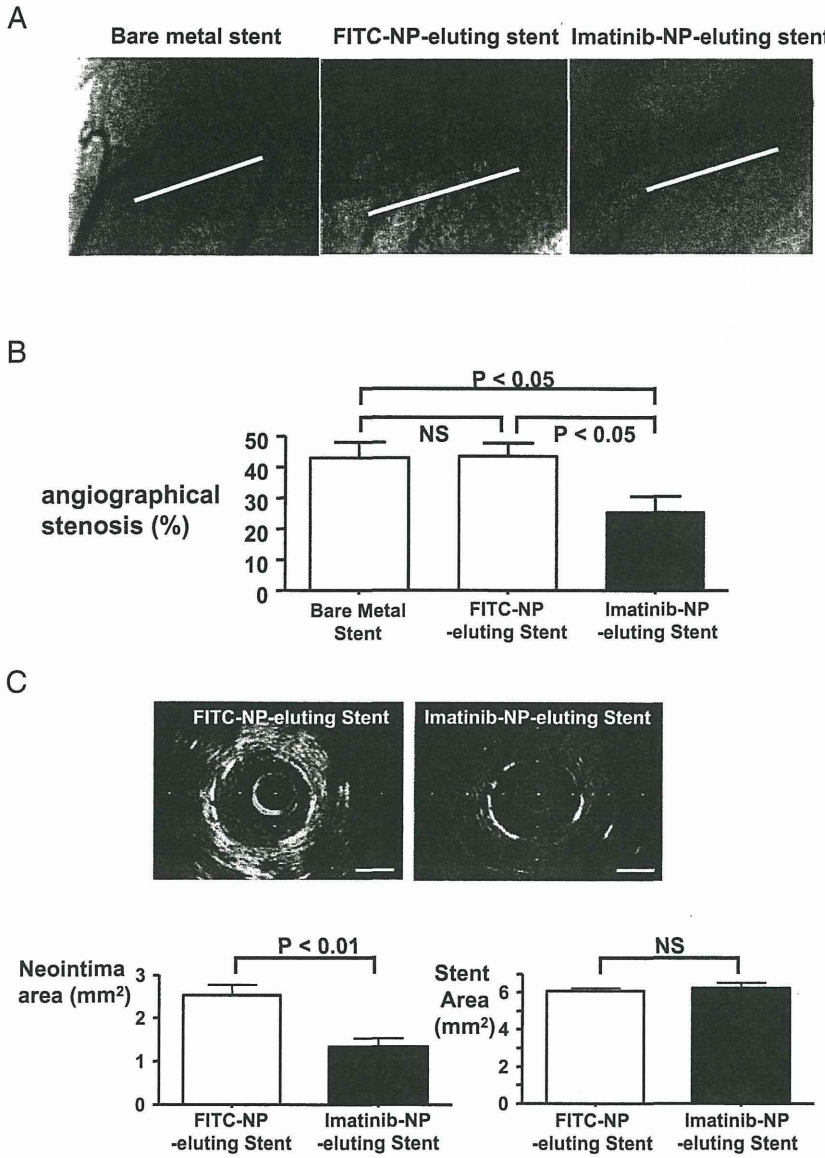

Fig. 3. Coronary arteriography and in-stent stenosis 4 weeks after stent implantation.

A, Representative coronary arteriographic images of stented segments in the left anterior descending coronary artery in bare metal, FITC-NP-eluting, and imatinib-NP-eluting stent groups. White bars in the images denote stented segments.
B, Angiographically-examined in-stent stenosis in bare metal ($n=8$), FITC-NP-eluting ($n=9$), and imatinib-NP-eluting ($n=10$) stent groups.
C, Intravascular ultrasound cross-section images and the summary of neointima formation (neointima area and stent area) in FITC-NP-eluting ($n=7$) and imatinib-NP-eluting ($n=8$) stent groups. Bar = 1 mm.

the control bare metal and FITC-NP-eluting stent sites than in the imatinib-NP-eluting stent sites 4 weeks after stenting (**Table 1**). Thus, angiographically, in-stent stenosis was less in the imatinib-NP group than in the control and FITC-NP group (**Fig. 3A and B**).

Intravascular ultrasound imaging (IVUS) could be performed in FITC-NP ($n=7$) and imatinib-NP stent ($n=8$) groups, which demonstrated that the extent of neointima formation was significantly less at the imatinib-NP stent site than at the FITC-NP-stent site (**Fig. 3C**).

Histological analysis demonstrated that a signifi-

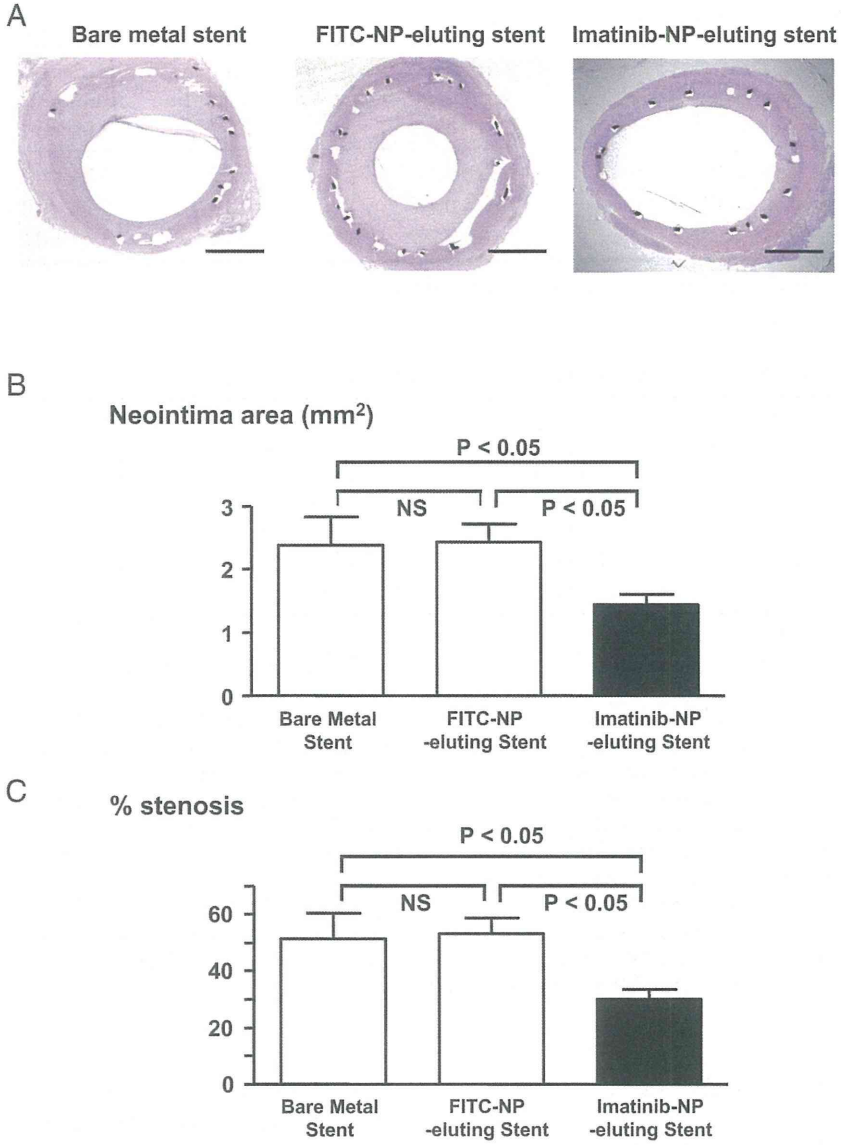

Fig. 4. Histopathological analysis of in-stent neointima formation 4 weeks after stent implantation.

A, Coronary artery cross-sections from the bare metal stent, FITC-NP-eluting stent, and the imatinib-NP-eluting stent groups. Tissue was stained with hematoxylin-eosin. Bar = 1 mm.

B, The neointima area at bare metal stents ($n = 8$), FITC-NP-eluting stents stents ($n = 9$), and the imatinib-NP-eluting stents ($n = 10$). NS = not significant. For statistical analysis, one-way ANOVA and Bonferroni's multiple comparison tests were performed.

C, The % stenosis [100 × (area of internal elastic lamia - neointima area)/area of internal elastic lamia] at bare metal stents, FITC-NP-eluting stents and the imatinib-NP-eluting stents. NS = not significant.

cant in-stent neointima formed similarly at the non-coated bare metal stent and FITC-NP-eluting stent sites. Quantitative analysis demonstrated a significant reduction in neointima formation at the imatinib-NP-eluting stent site (**Fig. 4**). In contrast, there were no significant differences in IEL and EEL areas among all 3 groups (**Table 2**). A semiquantitative histological scoring system demonstrated no significant difference in the injury score and inflammation score among the 3 groups (**Table 3**). Endothelial cell linings were